Periodica Polytechnica Civil Engineering, 66(4), pp. 1262–1277, 2022

Analysis of FGM Cantilever Beams under Bending-torsional Behavior Using a Refined 1D Beam Theory

Ilies Guendouz[1*], Mourad Khebizi[2], Hamza Guenfoud[3], Mohamed Guenfoud[1]

[1] Civil Engineering and Hydraulic Laboratory, University of 8 Mai 1945, P.B. 401, Guelma, 24000, Algeria
[2] Department of Civil Engineering, Mentouri University of Constantine, P.B. 325, Route de Aïn-El-Bey, Constantine, 25000, Algeria
[3] Department of Civil Engineering, University of Abbes Laghrour Khenchela, P.B. 1252, Route de Batna Khenchela, Khenchela, 40000, Algeria
[*] Corresponding author, e-mail: guendouz.ilies@univ-guelma.dz

Received: 04 June 2022, Accepted: 28 August 2022, Published online: 07 September 2022

Abstract

The static bending-torsion problem of functionally graded cantilever beams is studied using a refined 1D/3D beam theory (Refined beam theory RBT and Refined beam theory with distortion modes RBT*) built on the 3D Saint-Venant (SV) solution. In these theories, the displacement models include Poisson's effects, out-of-plane deformations and distortions. For a given section, the sectional displacement modes are derived from the computation of the particular 3D Saint-Venant's solution. These modes, which reflect the mechanical behavior of the cross-section, lead to a beam theory that actually corresponds to the cross-section type in terms of shape and material. In addition, the models take into account edge effects to predict a 3D solution in a larger internal region to better describe the overall behavior of FGM beams. The models examined are implemented on the CSB (Cross-Section and Beam Analysis) tool. It is based on the RBT/SV (Refined Beam Theory based on the 3D SV's solution) theory of FGM beams. The mechanical and physical characteristics of the FGM beams vary continuously, according to a power-law distribution, through the thickness of the beams. The numerical and 3D results obtained with homogeneous and FGM beams are systematically compared with other models in the literature and those provided by the full Saint-Venant beam theory (SVBT) calculations.

Keywords

FGM, cross-section, refined beam theory, bending-torsional, distortional modes

1 Introduction

Functionally graded materials (FGMs) are among the most widely used and widespread inhomogeneous complex materials during the past few decades, due to their great advantages of microstructures, spatially structure, and properties through the irregular distribution of the reinforcement phase [1]. As a new composite material, functionally graded materials have a tremendous ability to reduce stress concentration and alleviate thermal stress, these unique features make it a preferred material for use in various new structures. There are many uses of functionally graded materials in many fields, e.g., the automotive and aircraft sectors, in the field of civil and mechanical engineering, as well as in various elements of machines [2]. The mechanical properties of functionally graded materials differ through a continuous gradient of two or more components (often between metal and ceramic) in one direction (through length or thickness) or two directions (length and thickness). Various and efficient structural finite elements (beams, plates, and shells) require suitable homogenization procedures in order to reach the maximum rigidity of the shear, bending, transverse, and torsional shear properties [3, 4]. It should be noted that a huge number of papers dealing with modeling and simulation of the static and dynamic problems of functionally graded material beams can be found in many pieces of literature's works.

The overall list of studies devoted to the analysis of functionally graded materials (FGMs) structures subjected to various loadings is given in a paper's review by Birman and Byrd [5]. Based on the Euler–Bernoulli-Vlasov theory, the nonlinear flexion behavior of functionally graded beams (I section, and channel-section) is studied by Lanc et al. [6]. Chakraborty et al. [7] developed a new beam element based on the first-order shear deformation theory, this element aims to study the thermal

Cite this article as: Guendouz, I., Khebizi, M., Guenfoud, H., Guenfoud, M. "Analysis of FGM Cantilever Beams under Bending-torsional Behavior Using a Refined 1D Beam Theory", Periodica Polytechnica Civil Engineering, 66(4), pp. 1262–1277, 2022. https://doi.org/10.3311/PPci.20595

elastic behavior of functionally graded beam structures. Wu et al. [8] studied functionally graded and heterogeneous beams using the semi-inverse method in order to find solutions to the dynamic equation. Rahmani et al. [9] presented different beam theories to study bending, free vibration and buckling of functionally graded beam materials. where the finite element method is used to solve the problems numerically. Ying et al. [10] used the two-dimensional elasticity theory to study the vibration and bending behavior of the FGM beam. Barretta et al. [11] presented a torsion analysis for functionally graded beams (FGMs) with heterogeneous cross-sections based on Saint-Venant beam theory. Giunta et al. [12] used the classical (Euler Bernoulli and Timoshenko) and advanced theories to study the functionally graded beams with changing material properties in one or two directions. Kadoli et al. [13] focused on the theory of high-order shear deformation for the application of the displacement field in order to study the static analysis of functionally graded beams under ambient temperature. Kang and Li [14] used large and small deformation theories to study a functionally graded cantilever beam subjected to a force on the free end according to the non-linearity power-law. Li et al. [15] presented a new beam model to study the nonlinear bending behavior of a functionally graded two-dimensional beam based on the Euler–Bernoulli beam theory. Kien and Gan [16] used the finite element method to study the large deflections of tapered functionally graded beams. They also used a first-order shear beam element to interpolate the transverse displacement and rotation. Sankar [17] provided an elasticity solution for functionally graded materials beams under static transverse loads based on the assumption that material characteristics fluctuate exponentially along the thickness direction. Based on the first-order shear deformation theory, Benatta et al. [18] presented a static analysis of FG short beams including the problem of warping and shear deformation effects. Nguyen et al. [19] investigated the dynamic behavior of non-uniform functionally graded materials Timoshenko beams subjected to a moving load with varying speeds. Sindkhedkar et al. [20] based on Vlasov's theory and first-order shear deformation theory studied the flexural behavior of functionally graded thin beams. Li et al. [21] discovered analytical relationships between the bending solutions of FGM Timoshenko beams and those of homogenous Euler- Bernoulli beams. Nguyen et al. [22] investigated the FGM beams (mono-symmetric I and channel section) using Vlasov's thin-walled beam theory and Euler-Bernoulli beam theory. The minimal potential energy concept was used to generate governing equations. Furthermore, they looked at three different types of material distribution and compared the outcomes for each. Yang [23] used a finite element model based on quasi-3D theory in order to study the static behavior of an FG sandwich beam. Under a uniformly distributed load, several symmetric and non-symmetric sandwich beams with FGMs were considered. concluded that the influence of normal strain was significant and should be taken into account in the static behavior of sandwich beams. Şimşek [24] studied the vibration characteristics of bi-directional Timoshenko functionally graded beams (BDFGMs) under different boundary conditions. Nguyen et al. [25] investigated the effect of bending behavior of functionally graded materials beams (FGMs) by developing a beam element based on quasi-3D beam theory. Boutahar et al. [26] presented an analysis of the curved vibrational behavior of functionally graded thick beams based on the Refined Beam Theory (RBT). Madenci [27] used variational methods to analyze the thick-thin FGM beams using the shear deformation theory. Also, the mixed-finite element method (FEM) is employed to obtain a beam element. Garg et al. [28] presented the refined layer-wise theory to treat the bending of functionally graded materials beam using exponential and sigmoidal laws. Demirbas et al. [29] used refined beam models according to the Carrera unified formulation in order to estimate the stress of functionally graded beams. Zghal and Dammak [30] developed a high-order shear formulation according to a double field of displacements and stresses to analyze the vibrational behavior of functionally graded materials beams. Ziou et al. [31] developed a high-order shear deformation theory that simulates Timoshenko's beam theory to study FGM beam under static loading. Nguyen et al. [32] used a beam element to analyze the flexural-torsional stability of thin-walled open sections with FGM beams based on different types of distributions. Guendouz et al. [33] studied bending-torsional behavior of FGM cantilever beam using a refined beam theory (RBT). Khebizi et al. [34] presented the mechanical behavior of FGM beam using the 3D Saint-Venant's beam theory. this theory includes the 3D displacement modes of the cross-section which reflect Poisson's effects and out-of-plane warping.

The use of FGM beams is a real trend in many engineering applications. It is not easy to design this type of composite material (FGM), as the difficulty lies in predicting and understanding their mechanical behavior, especially when FGM beams are embedded (open, closed, thin-walled).

This requires the development of a realistic general beam theory that takes into account 3D effects while using a 1D model with cross-sectional deformation modes (distortional modes), in terms of displacement and stress (especially).

In the present paper, we examine the bending-torsional and torsional behavior of beams made of functional gradient materials (FGMs) using different beam theories (advanced and classical). The material properties of the FGM beam vary continuously across its thickness according to a power-law distribution. Two FGM beams (I-section and square-section) were adopted in this study, fixed on one side and free on the other side. These beams are subjected to bending-torsion and torsion actions, respectively, applying identical loads on the free end. These kinetic models include the own 3D displacement modes of the cross-section which reflect in, and out-of-plane warping extracted from the 3D SV's solution.

2 Functionally graded materials (FGMs)

The properties of functionally graded materials (FGMs) beams vary continuously through the thickness according to the volume fraction of the constituent materials (metal and ceramic). The power-law (P-FGM) most commonly describes differences in the properties of materials [34–37].

Based on the power-law distribution function, Young's modulus $E(y)$ [34, 38], can be expressed as:

$$E(y) = E_b + (E_t - E_b) \times \left(\frac{2y + h}{2h} \right)^P . \quad (1)$$

E_t and E_b are Young's modulus on the top and bottom FGM beam surface, y is the vertical axis of inertia of the section, P and h are the exponent of the power-law and beam's thickness, respectively.

For the exponential distribution (E–FGM), the young's modulus is given by Khebizi et al. [34].

$$E(y) = A \times e^{B \times \left(y + \frac{h}{2} \right)}, \text{ where } A = E_b, B = \frac{1}{h} \ln\left(\frac{E_t}{E_b}\right) \quad (2)$$

Several studies have shown that the Poisson's ratio has a significantly weaker effect on the deformation than Young's modulus [34, 35, 39].

Figs. 1 and 2 illustrate the variation of Young's modulus through the thickness of the FGM beam obtained by P-FGM and E-FGM, respectively. We can see from Figs. 1 and 2 that the graded material varies from the bottom (ceramic) to the top (metal) continuously through the thickness, followed by the change in material properties for different power-law indices.

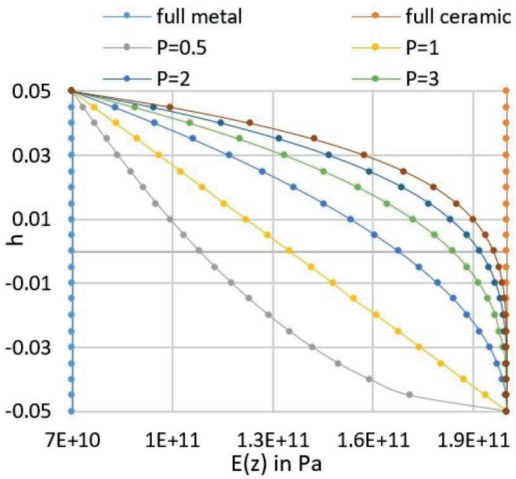

Fig. 1 Variation of Young's modulus through the thickness according to power-law (P–FGM)

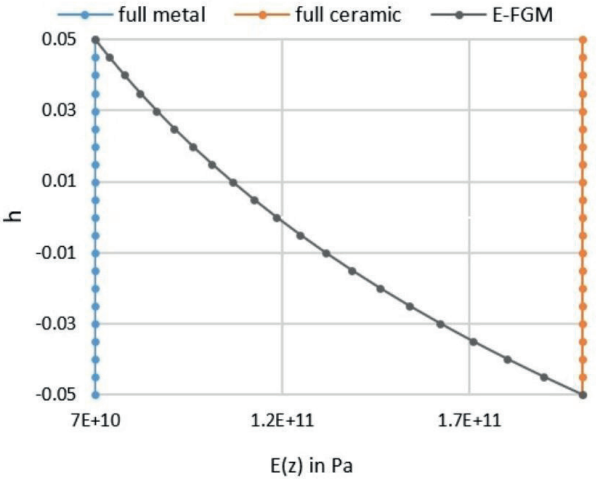

Fig. 2 Variation of Young's modulus through the thickness according to exponential distribution (E–FGM)

3 Formulation of the problem

3.1 The refined beam theory (RBT) built on Saint-Venant's solution

RBT is a higher-order beam theory mainly based on the 3D SV's solution to account for most of the edge effects, where only the 6 SV's cross-section deformation modes are taken into account and which concern to the 6 internal efforts [T_x, T_y, N, M_x, M_y, M_t].

3.1.1 The reference problem

We start with the cantilever beam shown in Fig. 3 with a constant (unspecified) section S, z-axis, and length L. The beam, clamped in $z = 0$, is subjected to a body loading $\boldsymbol{f}$ and a surface force $\boldsymbol{H}$ at $z = \mathrm{L}$. A point M is specified by $M = ZZ + \boldsymbol{GM}$, where G is the center of inertia of the cross-section and GM belongs to S. Finally, [x, y] are indicated by the axes of inertia of the section. (vectors and tensors are noted in bold-italic characters)

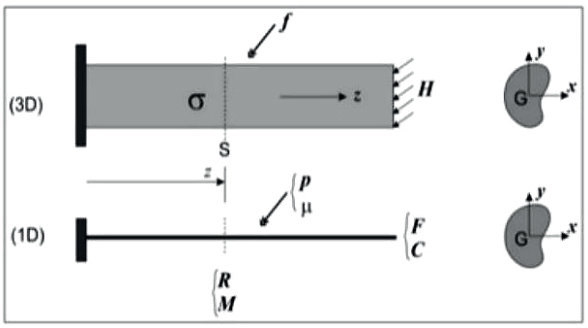

Fig. 3 Three-dimensional beam and one-dimensional modelling

3.1.2 RBT displacement model

The displacement field of a coordinate point (x, y, z) belonging to the beam is given as follows:

$$\xi(x,y,z) = \overbrace{\boldsymbol{u}(z)+\boldsymbol{\omega}(z)\wedge\boldsymbol{X}}^{\text{rigid montion of the section}} + \overbrace{\sum_{k=1}^{p}\eta_k(z)\boldsymbol{M}^k(x,y)}^{enrichment}. \quad (3)$$

The analytical model Eq. (3), expressing the total displacement of a point belonging to the beam, is a combination of a rigid solid motion (the first part of Eq. (3) depends only on the longitudinal z-coordinate of the point) and a pure deformation (the second part of Eq. (3) depends on the 3 coordinates x, y and z of the considered point, x and y are the transverse coordinates of the point and z the longitudinal coordinate). The deformation modes of the section are obtained numerically (by finite elements) following a modal analysis (free vibration) of the section.

The first 6 modes are the main modes that must be used, while the upper modes are used according on the higher-order theory used. According to the length of the beam, a classical discretization by finite elements with two nodes is considered.

The first term represents the rigid motion of the section. Where ($\boldsymbol{u}$, $\boldsymbol{\omega}$) are the cross-sectional displacement (translation and rotation), $\boldsymbol{X}$ the in-section vector position. The second term is used to deform the section depending on the modes $\boldsymbol{M}^k(x, y)$ (the displacement field of the cross-section), η_k additional Kinematic parameters (KP) associated to the set of P sectional modes $\boldsymbol{M}^k$ considered to be defined, where each parameter $\eta_k(z)$ determines the amplitude of the mode $\boldsymbol{M}^k(x, y)$.

The kinematic parameters $\{u_x, u_y, u_z, \omega_x, \omega_y, \omega_z, \ldots, \eta_k\}$ related to the general model constitute $(6 + P)$ degrees of freedom of the section's motion: the 3 translations (u_x, u_y, u_z) are used to control the translations of the section, the 3 rotations $(\omega_x, \omega_y, \omega_z)$ are used to control the rotations of the section and P$\{\eta_k\}$ associated to the sectional modes $\boldsymbol{M}^k$ is used to control the deformation modes of the section.

The difficulty in formulating a higher displacement model is lies selecting the $\boldsymbol{M}^k$ modes, in terms of numbers (not too large) and in terms of selection (most relevant to describing section deformation) (Naccache and El Fatmi [40]).

The one-dimensional equilibrium equations of the beam

The equations governing the equilibrium of the beam according to RBT are:

Equilibrium equations (1D):

$$\left.\begin{aligned} \boldsymbol{R}' + \boldsymbol{p} &= 0 \\ \boldsymbol{M}' + \boldsymbol{x}\wedge\boldsymbol{R} + \boldsymbol{\mu} &= 0 \\ A^{k'} - A_s^k + k^k &= 0\,(\forall k) \end{aligned}\right\}, \quad (4)$$

where $(\cdot)'$ denotes the derivative with respect to z.

The behavior law (1D):

$$\begin{bmatrix} \boldsymbol{R} \\ \boldsymbol{M} \\ \vdots \\ A_s^k \\ A_k \\ \vdots \end{bmatrix} = \boldsymbol{\Gamma}_{RBT} \begin{bmatrix} \boldsymbol{u}' + \boldsymbol{z}\wedge\boldsymbol{\omega} \\ \boldsymbol{\omega}' \\ \vdots \\ \eta_k \\ \eta_k' \\ \vdots \end{bmatrix}, \quad (5)$$

where A_s^k and A_k are internal efforts associated with $\boldsymbol{M}^k$ (Elfatmi [41]) and defined by:

$$\left.\begin{aligned} A^k &= \int_S \left(\sigma_{xz}M_x^k + \sigma_{yz}M_y^k + \sigma_{zz}M_z^k\right)dS \\ A_s^k &= \int_S \left(\begin{aligned} &\sigma_{xx}M_{x,x}^k + \sigma_{yy}M_{y,y}^k + \sigma_{xy}\left(M_{x,y}^k + M_{y,x}^i\right) \\ &+\sigma_{xz}M_{z,x}^k + \sigma_{yz}M_{z,y}^k \end{aligned}\right)dS \end{aligned}\right\}, \quad (6)$$

where $[\sigma_{xx}, \sigma_{yy}, \sigma_{xy}, \sigma_{xz}, \sigma_{yz}, \sigma_{zz}]$ are the components of the stress tensor.

For the problem of the cantilever in Fig. 3, the boundary conditions (1D) are as follows:

$$\begin{aligned} &x = 0\,(\boldsymbol{u},\boldsymbol{\omega}) = (0,0) \text{ et } \{\eta\} = 0\,(\forall k), \\ &x = L\,[\boldsymbol{R},\boldsymbol{M}] = [\boldsymbol{F},\boldsymbol{C}] \text{ et } A^k = Q^k\,(\forall k), \end{aligned} \quad (7)$$

where $\boldsymbol{R}$ and $\boldsymbol{M}$ are the classical internal forces (1D): $\boldsymbol{R}$ resulting from internal actions and $\boldsymbol{M}$ moment of internal actions.

$$\left.\begin{aligned}\boldsymbol{R}&=\int_S \boldsymbol{\sigma}\cdot\boldsymbol{z}dS=\begin{bmatrix}T_x\\T_y\\N\end{bmatrix}\\ \boldsymbol{M}&=\int_S\left(\boldsymbol{X}\wedge\boldsymbol{\sigma}\cdot\boldsymbol{z}\right)dS=\begin{bmatrix}M_x\\M_y\\M_t\end{bmatrix}\end{aligned}\right\},\tag{8}$$

where the six components are the 6 classical internal efforts [T_x, T_y, N, M_x, M_y, M_t]: the shear forces, the axial force, the bending moments and the torsional moment, respectively.

The external 3D actions $\boldsymbol{f}$ and $\boldsymbol{H}$ are modelled, respectively, by the (1D) point [$\boldsymbol{P}$, $\boldsymbol{F}$] and linear [$\boldsymbol{p}$, $\boldsymbol{\mu}$] actions defined by:

$$\left.\begin{aligned}\boldsymbol{p}&=\int_S \boldsymbol{f}dS & \boldsymbol{P}&=\int_{S_L}\boldsymbol{H}dS\\ \boldsymbol{\mu}&=\int_S \boldsymbol{GM}\wedge\boldsymbol{f}dS & \boldsymbol{F}&=\int_{S_L}\boldsymbol{GM}\wedge\boldsymbol{H}dS\\ \kappa^k&=\int_S \boldsymbol{f}\cdot\boldsymbol{M}^k & Q^k&=\int_{S_L}\boldsymbol{H}\cdot\boldsymbol{M}^k dS\end{aligned}\right\},\tag{9}$$

where $\boldsymbol{p}$ and $\boldsymbol{\mu}$ represent linear density of force and linear density of moment, respectively. $\boldsymbol{P}$ is the force and $\boldsymbol{F}$ is the moment.

Where ($\boldsymbol{p}$, $\boldsymbol{\mu}$, $\boldsymbol{P}$, $\boldsymbol{C}$) indicates the classical 1D external forces related to translation and rotation, and (κ^k, Q^k) are new (or additional) generalized external forces related to the cross-section deformation modes $\boldsymbol{M}^k$.

Structural behavior: by using matrix notation, the tensor of deformations can be written $\mathcal{D}$:

$$[\boldsymbol{\varepsilon}](x,y,z)=\boldsymbol{B}(x,y)\mathcal{D}(z),\tag{10}$$

with

$$\boldsymbol{B}=\begin{bmatrix}0&0&0&0&0&0&\dots&M^k_{x,x}&0&\dots\\0&0&0&0&0&0&\dots&M^k_{y,y}&0&\dots\\0&0&0&0&0&0&\dots&M^k_{x,y}+M^k_{y,x}&0&\dots\\1&0&0&0&0&-y&\dots&M^k_{z,x}\ M^k_x&M^k_x&\dots\\0&1&0&0&0&x&\dots&M^k_{z,y}\ M^k_y&M^k_y&\dots\\0&0&1&0&-x&0&\dots&0&M^k_z&\dots\end{bmatrix},\quad \mathcal{D}=\begin{bmatrix}Y_x\\Y_y\\Y_z\\X_x\\X_y\\X_z\\\vdots\\\eta_k\\\eta'_k\\\vdots\end{bmatrix}\tag{11}$$

where $\mathcal{D}$ and represents the generalized 1D strain vector. If $\mathcal{T}$ is the corresponding generalized cross-sectional stress vector. The 1D elastic constitutive relation can be written $\mathcal{T}=\boldsymbol{\Gamma}\mathcal{D}$ where $\boldsymbol{\Gamma}$ defines the 1D structural rigidity operator. Also $(\cdot)_{,x}$ and $(\cdot)_{,y}$ denote the partial derivatives with respect to x and y.

$$\begin{bmatrix}\boldsymbol{R}\\\boldsymbol{M}\\\vdots\\A^k_s\\A_k\\\vdots\end{bmatrix}=\boldsymbol{\Gamma}_{RBT}\begin{bmatrix}\gamma\\\chi\\\vdots\\\eta_k\\\eta'_k\\\vdots\end{bmatrix}\tag{12}$$

The $\boldsymbol{\Gamma}$ operator can be derived from the identification

$$\int_S\left(\left[\varepsilon_I\right]^t\left[\boldsymbol{K}\right]\left[\varepsilon_J\right]\right)dS=\left[\mathcal{D}_I\right]^t\boldsymbol{\Gamma}\left[\mathcal{D}_J\right]$$

where (ε_I, $\mathcal{D}_I$) and (ε_J, $\mathcal{D}_J$) are any virtual strains. By introducing the expression for the deformations Eq. (10). The 1D behavior operator results are given by:

$$\boldsymbol{\Gamma}_{RBT}=\int_S\boldsymbol{B}^t(x,y)\boldsymbol{K}(x,y)\boldsymbol{B}(x,y)dS,\tag{13}$$

where $\boldsymbol{K}$ is the matrix (6 × 6) related to the elastic tensor.

The correspondent 3D solution

Consider [$\boldsymbol{u}^e(z)$, $\boldsymbol{\omega}^e(z)$, $\{\eta^e(z)\}$] the 1D equilibrium solution of a beam problem using the RBT model (RBT/SV). Conforming to the displacement model, the 1D solution permits a return to the 3D solution using the 3D displacement field:

$$\begin{aligned}\boldsymbol{U}^e(x,y,z)&=\boldsymbol{U}\left(\boldsymbol{u}^e,\boldsymbol{\omega}^e,\{\eta\}^e\right)\\&=\boldsymbol{u}^e(z)+\boldsymbol{\omega}^e(z)\wedge\boldsymbol{X}+\dots\eta^e_k(z)\boldsymbol{M}^k(x,y),\end{aligned}\tag{14}$$

which leads to the 3D stress tensor field.

$$\boldsymbol{\sigma}^e(x,y,z)=\boldsymbol{K}(x,y):\boldsymbol{\varepsilon}\left(\boldsymbol{U}^e(x,y,z)\right),\tag{15}$$

where $\varepsilon(\boldsymbol{U})=1/2(\nabla^t\boldsymbol{U}+\nabla\boldsymbol{U})$ denotes the strain tensor associated with $\boldsymbol{U}$. And ∇, $(\cdot)^t$ denote the gradient and the transpose operators, respectively.

The 3D stress field may also be given with respect to the internal forces:

$$\sigma^e_{\mathrm{RBT/SV}}=\left[\boldsymbol{K}\right](x,y)\mathbf{B}(x,y)\boldsymbol{\Gamma}^{-1}\mathcal{T}^e(z).$$

3.2 The refined beam theory using the distortion modes (RBT*)

In this work, an enhanced displacement model RBT* (El Fatmi [41], Naccache and El Fatmi [42]), also built on SV's solution. this model includes edge effects, where all available deformation modes are taken into account. In the RBT* model, the displacement model is given by:

$$U(x,y,z)=\overbrace{\boldsymbol{u}(z)+\boldsymbol{\omega}(z)\wedge\boldsymbol{X}+\sum_{i=1}^{6}\alpha_i(z)\boldsymbol{M}_{sv}^{i}(x,y)}^{\textit{shape of SVBT displacement}}+\sum_{j=1}^{m}\beta_j(z)\boldsymbol{D}_{v}^{j}(x,y), \tag{16}$$

where the enrichment part now contains the following sectional modes:

- $\boldsymbol{M}_{sv}^{i}$ are the 6 3D-SV's modes related to the 6 cross-section stresses *(*T_x, T_y, N, M_x, M_y, M_t*)* without (artificially) splitting them into in-plane modes and out-of-plane modes.
- $\boldsymbol{D}_{v}^{j}$ are additional modes (distortion modes), to be used if a thin/thick-walled cross-section is concerned or a high-contrast composite section. These modes are the first m shapes of 3D modes associated with the free vibration of the cross-section; they principally reflect the distortions of the cross-section.

Comment: All modes $\{\boldsymbol{M}_{sv}^{i}, \boldsymbol{D}_{v}^{j}\}$ are section specific modes; they reflect the physical nature of the cross-section (shape and material). It follows that the beam theory generated by the model is adapted to the nature of the section.

3.3 Cross-section analysis

3.3.1 Homogeneous isotropic case

The stiffness operator $\boldsymbol{\Gamma}$ (matrix 6 × 6) is used to solve and define a one-dimensional (1D) problem, which depends only on the nature of the cross-section (shape, material) (Khebizi et al. [34]). Where The flexibility operator is indicated by $\boldsymbol{\Lambda}=\boldsymbol{\Gamma}^{-1}$.

Structural flexibility is defined as follows:

$$\boldsymbol{\Lambda}=\begin{bmatrix}\frac{1}{GS_x}+\frac{y_c^2}{GJ} & \frac{-x_c y_c}{GJ} & 0 & 0 & 0 & \frac{y_c}{GJ}\\ \frac{-x_c y_c}{GJ} & \frac{1}{GS_y}+\frac{x_c^2}{GJ} & 0 & 0 & 0 & \frac{-x_c}{GJ}\\ 0 & 0 & \frac{1}{ES} & 0 & 0 & 0\\ 0 & 0 & 0 & \frac{1}{EI_x} & 0 & 0\\ 0 & 0 & 0 & 0 & \frac{1}{EI_y} & 0\\ \frac{y_c}{GJ} & \frac{-x_c}{GJ} & 0 & 0 & 0 & \frac{1}{GJ}\end{bmatrix} \tag{17}$$

x_c and y_c are the coordinates of the shear centre C, J is the torsional inertia, G is the shear modulus, S_x and S_y are the reduced sectional connected to the shear forces T_x and T_y. I_x is the inertia moment with relation to x, and I_y the inertia moment with relation to y. E is Young's modulus. The constants [S, I_x, I_y, J, S_x, S_y, x_c, y_c] are only determined by the nature of the cross-section (shape and material). They can be specified once and for all for a particular section.

$$\boldsymbol{\sigma}^{e}(x,y,z)=\begin{bmatrix}0 & 0 & \sigma_{xz}^{e}\\ 0 & 0 & \sigma_{yz}^{e}\\ \sigma_{xz}^{e} & \sigma_{yz}^{e} & \sigma_{zz}^{e}\end{bmatrix}, \tag{18}$$

where the axial stress (σ_{zz}^{e}) depends only on [N^e, M_x^e, M_y^e] and the shears stress (σ_{yz}^{e}, σ_{xz}^{e}) depends only on [T_x^e, T_y^e, M_t^e]. The axial stress which is linear combination of [N^e, M_x^e, M_y^e] is written as follows:

$$\sigma_{zz}^{e}(x,y,z)=N^{e}(z,y)\cdot\left(\frac{1}{A}\right)+M_x^{e}(z,y)\cdot\left(\frac{y}{I_x}\right)-M_y^{e}(z,y)\cdot\left(\frac{x}{I_y}\right). \tag{19}$$

The stress fields σ_i associated with [N^e, M_x^e, M_y^e] can be derived and which reduce to the axial stress by:

$$\boldsymbol{\sigma}^{3}(x,y)=\begin{bmatrix}0 & 0 & 0\\ 0 & 0 & 0\\ 0 & 0 & \frac{1}{A}\end{bmatrix}.N^{e},$$

$$\boldsymbol{\sigma}^{4}(x,y)=\begin{bmatrix}0 & 0 & 0\\ 0 & 0 & 0\\ 0 & 0 & \frac{y}{I_x}\end{bmatrix}.M_x^{e}, \tag{20}$$

$$\boldsymbol{\sigma}^{5}(x,y)=\begin{bmatrix}0 & 0 & 0\\ 0 & 0 & 0\\ 0 & 0 & -\frac{x}{I_y}\end{bmatrix}.M_y^{e}.$$

These fields (σ_i) are only based on the cross-section properties [A, I_x, I_y].

It should be mentioned that the SV's solution leads to the same analytical description of the axial stress in the case of an isotropic homogeneous beam.

The Shear stresses which are a linear combination of [T_x^e, T_y^e, M_t^e] are written as follows:

$$\sigma_{xz}^{e}(x,y,z) = f_x^x(x,y)\cdot T_x^e(z) + f_x^y(x,y)\cdot T_y^e(z) + f_x^t(x,y)\cdot M_t^e(z), \quad (21)$$

$$\sigma_{yz}^{e}(x,y,z) = f_y^x(x,y)\cdot T_x^e(z) + f_y^y(x,y)\cdot T_y^e(z) + f_y^t(x,y)\cdot M_t^e(z), \quad (22)$$

where the functions ($f_i^j(x, y) : f_x^x(x, y)$, $f_x^y(x, y)$, $f_x^t(x, y)$, $f_y^x(x, y)$, $f_y^y(x, y)$ and $f_y^t(x, y)$ depend on the cross-section nature (shape and material) and which, they can only be determined numerically (with the exception of the circular section for which these functions can be determined analytically).

Three-dimensional (3D) displacement field

For the case of the homogeneous and isotropic section. SV's solution for the 3D displacement field has been illustrated as follows:

- Normal effort and bending moments [N, M_x, M_y], only contribute to Poisson's ratio effects [$\boldsymbol{U}^3(x, y)$, $\boldsymbol{U}^4(x, y)$, $\boldsymbol{U}^5(x, y)$]. are thus planes (the component along z is zero).
- Shear forces and torsional moments [T_x, T_y, M_t], only contribute to warping [$\boldsymbol{U}^1(x, y)$, $\boldsymbol{U}^2(x, y)$, $\boldsymbol{U}^6(x, y)$]. They are therefore out-of-plane (their components, in relation to x and y, are zero).

3.3.2 Composite section

One-dimensional (1D) behavior law

There are many couplings between tension and bending-torsion in the composite section, due to the material being anisotropic. Besides, the stiffness operator Γ in a matrix (6 × 6) indicates the possibility that it is full. Also, every non-zero term out of the diagonal reflects a type of coupling. For the homogeneous case, the asymmetric cross-section results in coupling bending-torsional.

According to a composite section, the various stiffness constants are expressed as follows:

$\widetilde{G_y S_x}$ the shear force stiffness /x
$\widetilde{G_y S_y}$ the shear force stiffness /y
$\widetilde{E_y S}$ the axial stiffness
$\widetilde{E_y I_x}$ the bending stiffness /x
$\widetilde{E_y I_y}$ the bending stiffness /y
$\widetilde{G_y J}$ the torsional stiffness.

The cross-sectional constants involved in the constitutive relations are the six classical composite cross-sectional constants [$\widetilde{G_y S_x}, \widetilde{G_y S_y}, \widetilde{E_y S}, \widetilde{E_y I_x}, \widetilde{E_y I_y}, \widetilde{G_y J}$]. The cross-sectional constants are designated by these terms by analogy with the isotropic and homogeneous case; each term is to be considered as a symbol and is not separable (more details by El Fatmi and Ghazouani [43]).

Three-dimensional (3D) stress field

For each composite section, the components (σ_{xx}, σ_{yy}, σ_{xy}) of the stress field are not zero (Eq. (23)). In the homogeneous case, it is zero (Eq. (18)).

The variation in Poisson's ratio between materials is sufficient to produce stresses in the cross-section plane.

$$\boldsymbol{\sigma} = \begin{bmatrix} \sigma_{xx} & \sigma_{xy} & \sigma_{xz} \\ \sigma_{xy} & \sigma_{yy} & \sigma_{yz} \\ \sigma_{xz} & \sigma_{yz} & \sigma_{zz} \end{bmatrix} \quad (23)$$

Three-dimensional displacement field

In the homogeneous isotropic case, [N, M_x, M_y] lead only to Poisson's ratio effects, while [T_x, T_y, M_t] lead only to warping. in the composite case, any of the 6 internal forces (T_x, T_y, N, M_x, M_y, M_t) can be responsible for both Poisson's effects and out-of-plane warping [34].

3.4 Advantages of this model compared to other models

The Saint Venant or Timoshenko/Bernoulli beam theories are classical beam theories. It should be remembered that the Timoshenko/Bernoulli beam theories are based on simplifying assumptions. i.e., the starting point is a displacement model which supposes that the section is undeformable (they do not take into account beam cross-section deformation), and the 3D computation time is too heavy (a large number of finite elements). Saint Venant's beam theory follows from the 3D SV's solution, where the section is free to deform. It also owes its justification to the fact that the resolution according to the SV beam theory leads to the 3D SV's solution which represents, far from the edges, the exact 3D solution of the equilibrium of the beam (more details about beam models [44]).

RBT/SV is a higher-order beam theory built (mostly) on SV's solution; which allows it: to better satisfy the support conditions, better model the external actions, and find far from the edges the 3D SV's solution because the displacement model contains the shape of the displacement of the SV's solution; and to better account for edge effects, because the boundary conditions can be better satisfied (in terms of force and displacement). Finally, RBT can be seen as a very extended generalization of Vlasov's theory; this only concerns torsional warping for the special case of homogeneous and isotropic open thin sections,

whereas RBT/SV addresses any section (shape and material) and considers all types of section deformation (warping, Poisson's effects, distortions).

4 Numerical results and discussion

4.1 Numerical implementation

In this work, the theory of RBT/SV was introduced by a tool called CSB (Cross-section and Beam Analysis) (Naccache and El Fatmi [40]).

CSB is a numerical tool dedicated to the computation of beams with any cross-sectional shape, made of freely arranged isotropic or anisotropic materials. It is used to solve in the standard framework of linear elasticity and the equilibrium of a beam subjected to any loading and support conditions. CSB is proposed as a set of two complementary numerical tools CSection and CBeam:

- CSection calculates the mechanical characteristics of the cross-section ($\boldsymbol{M}_{sv}^{i}$) and a set of m distortion modes ($\boldsymbol{D}_{\gamma}^{j}$) by 2D finite element method (2D-FEM).
- CBeam uses these mechanical characteristics of the cross-section to calculate the beam by 1D finite element method (1D-FEM).

4.2 Bending analysis

In this section, in order to validate the current theory, we study a simply-supported FGM beam (L = 1.6 m, h = 0.1 m, b = 0.1 m) subjected to a uniformly distributed load q (see Fig. 4). Through the study this beam, the most important results obtained based on the 3D displacement fields are presented. The beam is composed of aluminum (AL: E_m = 70 GPa, v = 0.3); and Zirconia (Zero2: E_c = 200 GPa, v = 0.3). The mechanical properties of the FGM beam change through the thickness. The top surface of the beam ($y = +h/2$) is pure Aluminum, whereas the bottom surface of the beam ($y = -h/2$) is pure Zirconia.

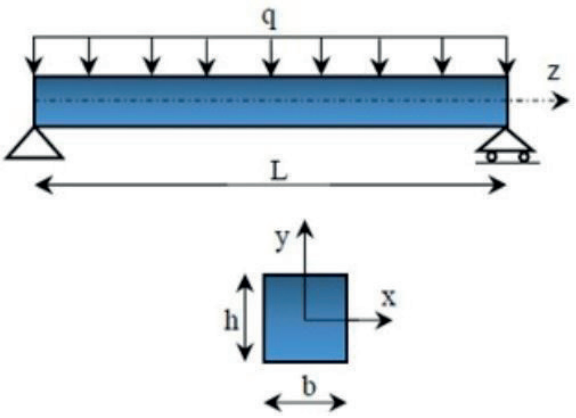

Fig. 4 Simply supported FGM beam

Figs. 5 and 6 show the non-dimensional transverse displacements (w/w_{static}) along the length of the FGM beam. The static deflection of a completely aluminium beam under uniformly distributed load is calculated as follows:

$$w_{\text{static}} = \frac{5 \times q \times L^4}{384 \times E_m \times I}. \tag{24}$$

The non-dimensional deflections (Fig. 5), obtained by a refined beam theory (RBT), are compared with those provided by Şimşek [45] (Fig. 6) using the higher-order shear deformation theory (HOSDT). It can be seen that the present results are in excellent agreement with HOSDT. It can also be seen that the deflection of full metal is greater than that of full ceramic, this can be explained by the fact that Young's modulus of ceramic is higher than that of metal. The non-dimensional deflection of the FGM beam ($P \neq 0$) is between those of the metal and ceramic beams. For the FGM beam, the non-dimensional transverse deflection decreases as the power-law exponent P increases. This is due to the fact that an increase in the power-law exponent leads to a decrease in the bending stiffness of the beam.

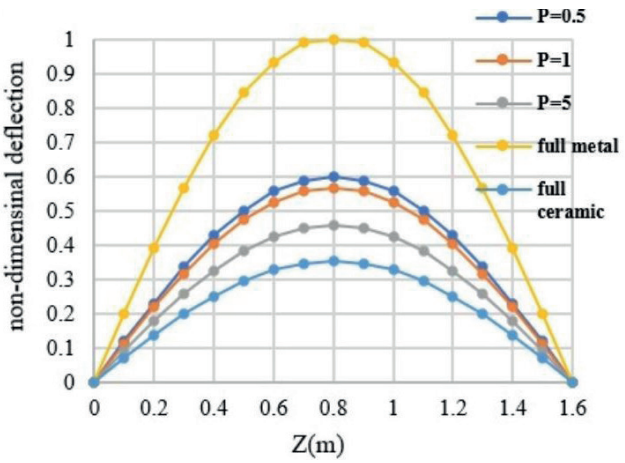

Fig. 5 Non-dimensional deflections distributions by RBT

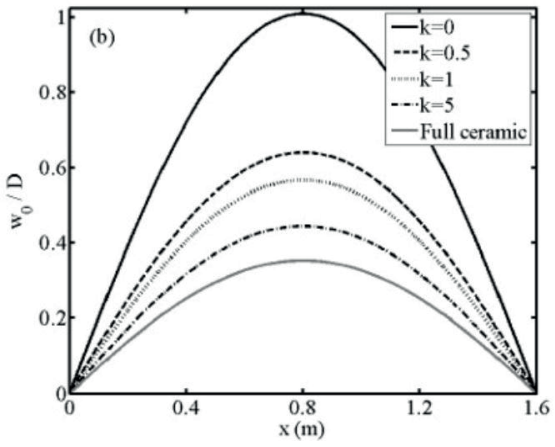

Fig. 6 Non-dimensional deflections distributions by Şimşek [45]

The axial stresses σ_{zz} are computed at the mid-span of the beam. The axial stress field obtained by 3D-RBT, is shown in Figs. 7 and 8. The shape of the 3D stress distribution is plane in the homogeneous case and passes through the middle axis of the cross-section while in the FGM beam it is not plane and does not pass through the middle axis of the cross-section.

Fig. 9 shows the distribution of non-dimensional axial stress through the thickness in mid-span of the FGM beam for different values of *P*. The results obtained with RBT show good agreement with those obtained with HOSDT by Şimşek [45] Fig. 10.

The axial stress is normalized by:

$$\bar{\sigma}_{zz} = \frac{\sigma_{zz} \times b \times h}{q \times L}. \quad (25)$$

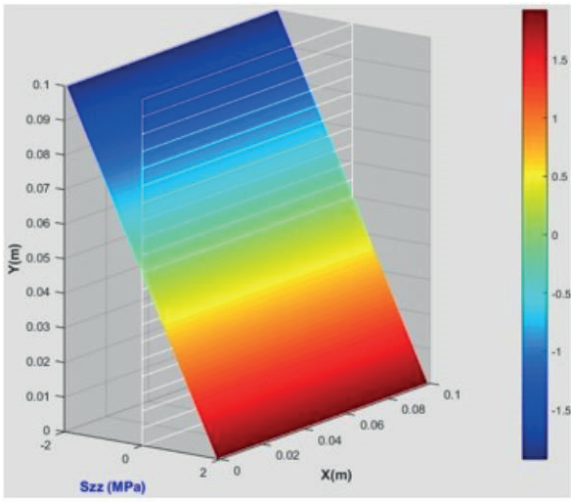

-1.924e6 Pa ≤ σ_{zz} ≤ 1.924e6 Pa

Fig. 7 (a)Axial stress distributions obtained by RBT ($P = 0$)

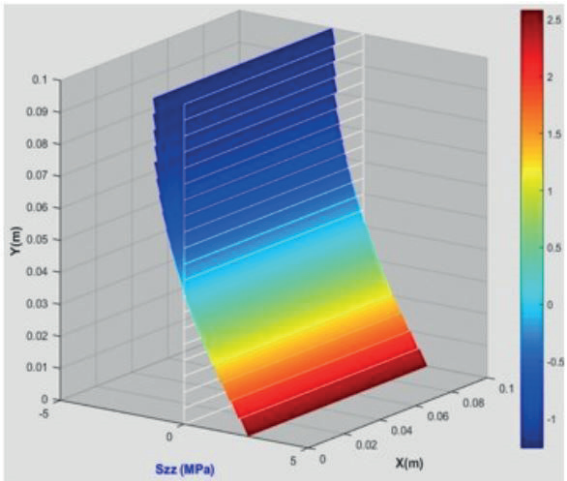

-1.260e6 Pa ≤ σ_{zz} ≤ 2.581e6 Pa

Fig. 8 (b)Axial stress distributions obtained by RBT ($P = 5$)

In Fig. 9 we can see that the axial stress distribution is only linear for full metal, but for other cases ($P \neq 0$) the axial stress distribution is not linear, and also the tensile stress values are greater than the compressive stresses in the case of FGM beam. on the other hand, we can note for the full metal, the value of axial stress is zero (σ_{zz}) at the mid-plane ($h/y = 0$), while for the other cases ($P \neq 0$) the axial stresses are not zero. This is due to the variation of the Young's modulus across the thickness of the FGM beam.

4.3 Bending-torsional analysis

In order to illustrate the performance of RBT/SV and the numerical tools CSection and CBeam, the most important 1D/3D results are given based of 3D displacement fields, in the inner region and near the edge of the beams. In order to compare the results of the different theories,

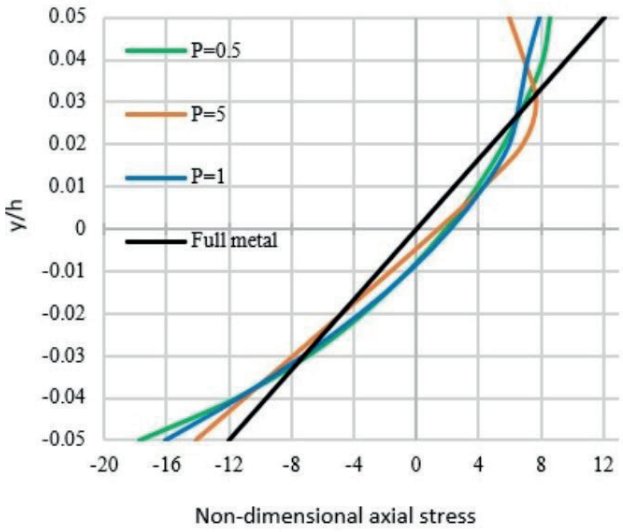

Fig. 9 Non-dimensional deflection obtained by RBT

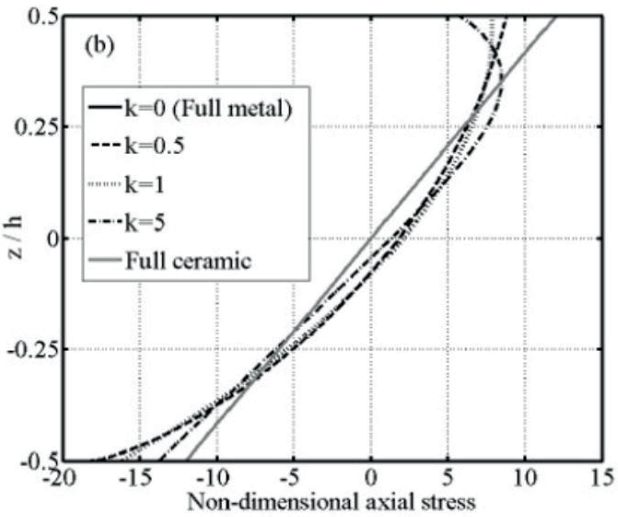

Fig. 10 Non-dimensional deflection obtained by Şimşek [45]

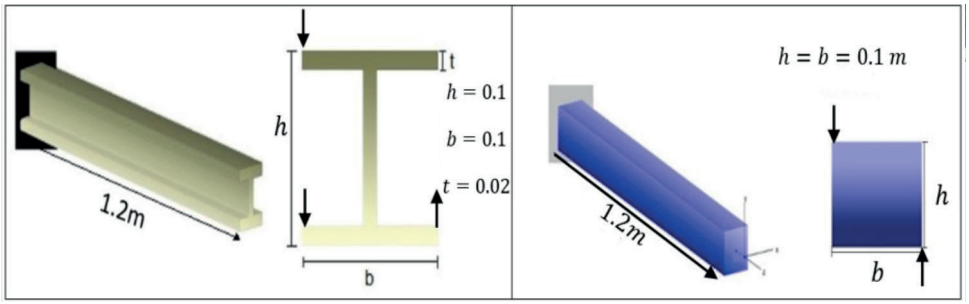

Fig. 11 FGM beams and sections description

we studied the cantilever FGM beams shown in Fig. 11. The first beam (I-section) is subjected to bending-torsional with three loads, for the second beam (square-section) it is subjected to torsional behavior resulting from two loads, all these loads are identical (1KN Per-Force) and applied at the free end of the beams (see Fig. 11). These beams are composed of aluminum (AL: E_m = 70 GPa, v = 0.3); and Zirconia (Zro2: E_c = 200 GPa, v = 0.3). The mechanical properties of FGM beams change through their thickness according to power-law and exponential distribution as shown in Figs. 1 and 2. The top surface of the beams ($y = + h/2$) is pure aluminum, whereas the bottom surface of the beams ($y = - h/2$) is pure zirconia.

4.3.1 Cross-section analysis

By using the CSection tool, 2D-FEM analyses of FGM beam cross-sections are performed. This tool provides for each section: the six cross-section modes ($\boldsymbol{M}_{sv}^{i}$) and a set of m distortion modes ($\boldsymbol{D}_{v}^{j}$) related to the natural vibration of the section.

Fig. 12 presents the six (6) transverse modes [T_x, T_y, N, M_x, M_y, M_t] associated with the classical transverse stresses of each section. the deformation modes in red color indicate the Poisson's effects related to the axial force (N) and the bending moments (M_x, M_y), while the deformations in blue color indicate the out-of-plane warpings related to the shear forces (T_x, T_y) and the torsional moment (M_t). In addition, certain additional sectional distortions are considered for I-Section and square-section: 10 in-plane (pink color) and 5 out-of-plane (blue color) shown in Fig. 13.

4.3.2 1D/3D results

FGM cantilever beam (I-section)

The analysis performed focuses on the effect of embedding on 3D stresses and the general behavior of the FGM beam. Table 1 shows the maximum transverse deflection of the cantilever beam (I-section) for different values of Power Law exponent, using the different theories. The deflection of the metal beam (P = 0) is found to be higher than the deflection of the ceramic beam ($P \rightarrow \infty$). This is illustrated by the fact that the Young's modulus of ceramic is greater than that of metal. For the FGM beam, the deflection is located between the deflections of metal and ceramic beams. Consequently, when the power-law exponent P is increased, the transverse deflection decreases in the case

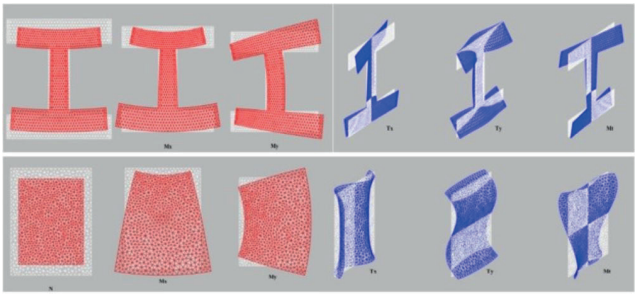

Fig. 12 Cross-sections deformations: Poisson's effects (N, M_x, M_y) and out-of-plane warpings (T_x, T_y, M_t) for the FGM sections (for P = 1)

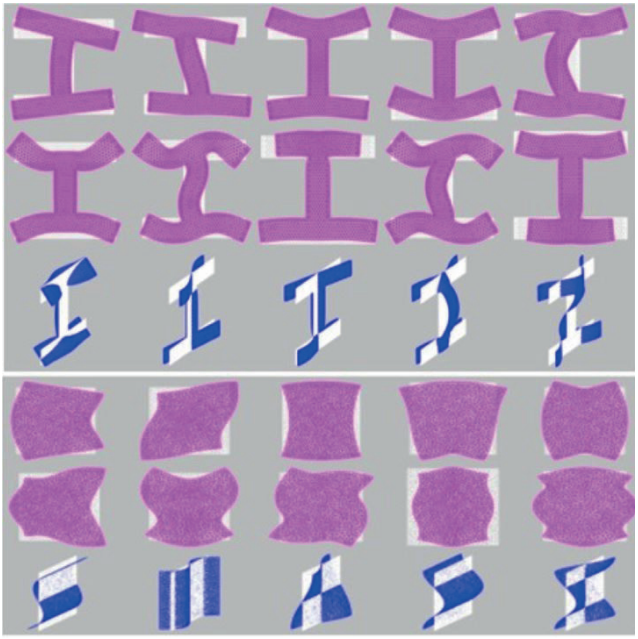

Fig. 13 Cross-section deformations: distortions modes $\boldsymbol{D}_{v}^{j}$ of the FGM sections (for P = 1)

Table 1 The maximum transverse deflection of an FGM cantilever beam (I-section) for various values of the power law exponent (mm)

Power-low Exponent	RBT	RBT*	SVBT
Full metal	1.2074	1.2081	1.2207
$P = 0.5$	0.7713	0.7714	0.7799
$P = 1$	0.7255	0.7259	0.7336
$P = 2$	0.6705	0.6709	0.6780
$P = 3$	0.6384	0.6390	0.6435
$P = 4$	0.6120	0.6124	0.6188
$P = 5$	0.5934	0.5937	0.6000
Full ceramic	0.4226	0.4228	0.4273

Table 2 Maximum torsional rotation of FGM cantilever beam (I-section) for various values of the power law exponent (rad 10-3)

Power-low Exponent	RBT	RBT*	SVBT
Full metal	8.1096	8.1372	9.2776
$P = 0.5$	4.7417	4.7589	5.3371
$P = 1$	4.2986	4.3159	4.8557
$P = 2$	3.9397	3.9547	4.4434
$P = 3$	3.7698	3.7855	4.2534
$P = 4$	3.6698	3.7855	4.1445
$P = 5$	3.6008	3.6832	4.0708
Full ceramic	2.8383	2.8480	3.24471

of the FGM beam. This is explained by an increase in the exponent of the power-law resulting in an increase in the bending rigidity of the FGM beam. It can also be seen that the value of the transverse deflection of the SVBT is comparatively higher than the other theories.

The maximum torsional rotation for an FGM cantilever beam depending on the different theories is given in Table 2. We notice an approximate similarity of the RBT, RBT* values, and a small difference to the SVBT theory. According to the deflection and torsional rotation for the FGM cantilever beam, we conclude that the RBT, RBT* behavior is stiffer than expected by SVBT.

Systematically, the comparison between the theories was carried out out by considering the main stress components for the FGM beam, the axial stress σ_{zz}, and the shear stress modulus $\tau = \sqrt{\tau_{xz}^2 + \tau_{yz}^2}$ in the different regions of the beam. Fig. 14. shows the axial stress fields at the embedding and in the mid-span of the beam, both for the homogeneous and FGM beam models. The results obtiened by SVBT are quite different from RBT and RBT* at embedding, while they converge at the mid-span of the beam. In addition, it can be seen that the axial stress distribution for the homogeneous case is linear. it shows that the axial stresses of the SVBT due to bending only, while for the FGM beam, the axial stress is nonlinear. similarly, the axial stresses of RBT and RBT* are very different from those obtained by the SVBT. Moreover, the difference results from the effect of the bending-torsion stress (clearly the torsion is important) resulting from the enrichment of the displacement field of RBT models. For the FGM beam

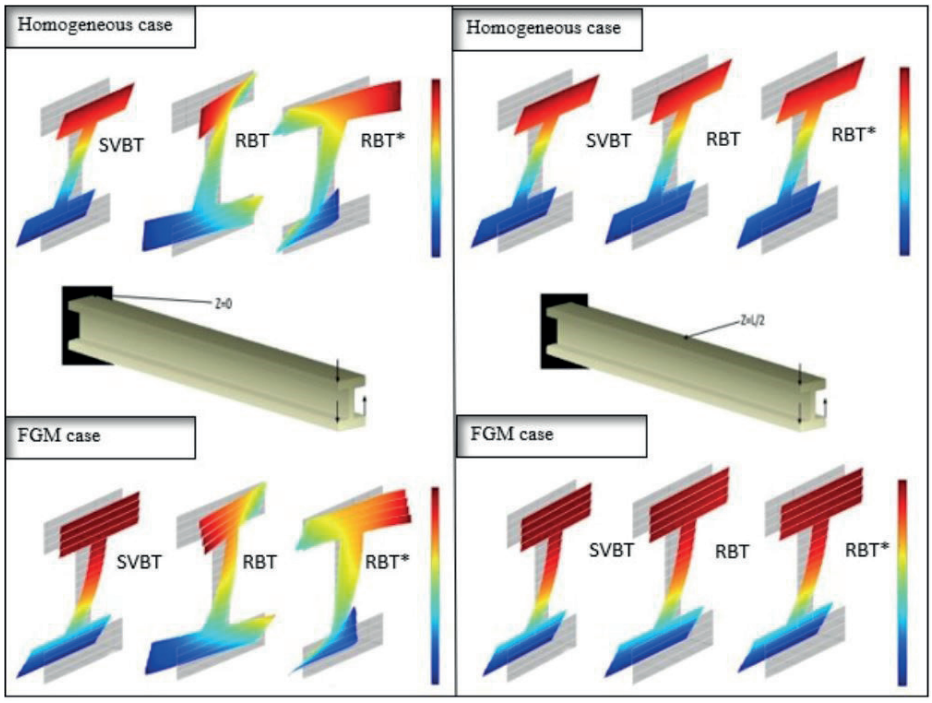

Fig. 14 Axial stresses distributions at embedding ($Z = 0$) and at mid-span ($Z = L/2$). Comparison of RBT, RBT* and SVBT

$P \neq 0$, the axial stress distribution is nonlinear and does not pass along the neutral axis (the line passing the Z-axis of the center of gravity). This is caused by the variation of Young's modulus in the thickness of the FGM beam.

Fig. 15. shows the variations of the axial stress (σ_{zz}) along the span for 2 points, A and B, that belong to the top flange of the FGM beam. The results as shown in Fig. 15 have been obtained using the present assumption, i.e., a non-deformable cross-section at the embedding for the SVBT and deformable for RBT and RBT*. It can be seen a large difference between the stress results of the three theories at the embedding level, and a convergence between the results is seen far from the embedding (The internal effect propagates over a distance of about $d \approx L/2$). If the section is taken as undeformable for both RBT and RBT*, the same results as for SVBT are found. we can see that RBT and RBT* take into account edge effects in order to predict a 3D solution in a larger internal region to better describe the overall behaviour of the beam. In SVBT, the 3D solution is an integral part and it describes the correct solution in the internal region of the beam.

Fig. 16 displays the comparison between the shear stress distributions at the embedding ($Z = 0$) and ($Z = L$). One can see that the shear stress fields are definitely different in terms of shape and materials for the three theories in the embedding area ($Z = 0$). The results of the shear stresses

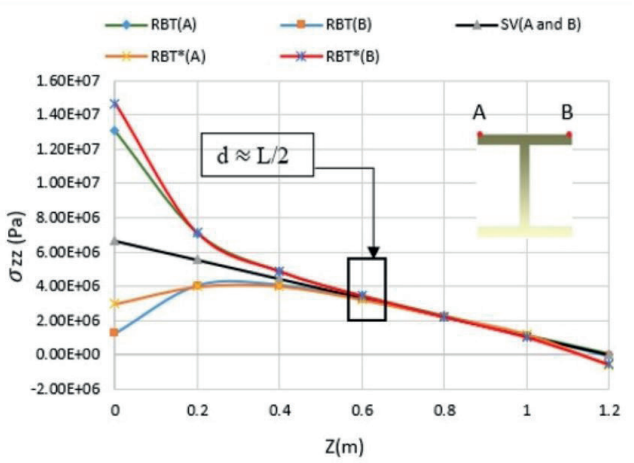

Fig. 15 Axial stress variations along the FGM beam for two points (A and B) belonging to the upper flange. Comparison of RBT, RBT* and SVBT

given by the SVBT are based on the shear force (T_y) and the torsional moment (M_t). The deformations avoided in the case of RBT and RBT* at the embedding level ($Z = 0$), led to totally different shear stresses than those given by SVBT. Far from the embedding ($Z \neq 0$), the shear stress results are similar for SVBT and RBT but different for RBT* (Some differences can be observed in the locations designated by the circles in Fig. 16). This is due to the enrichment of the displacement field through higher modes (additional deformation modes "distortion modes") Eq. (16).

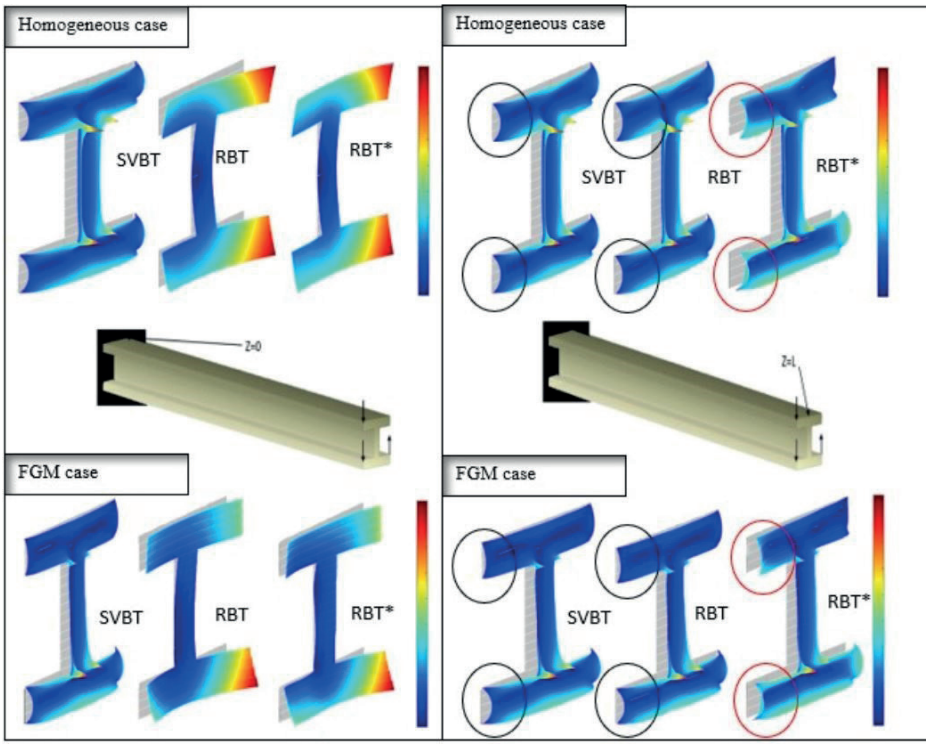

Fig. 16 Shear stresses distributions at embedding ($Z = 0$) and free end ($Z = L$). Comparison of RBT, RBT* and SVBT

Table 3 Maximum rotation of FGM cantilever beam (with square-section) for various values of the power law exponent (rad 10^{-3})

power-low exponent	RBT	RBT*	SVBT
full metal	0.3163	0.3163	0.3171
$P = 0.5$	0.2120	0.2121	0.2129
$P = 1$	0.1695	0.1695	0.1699
$P = 2$	0.1489	0.1489	0.1493
$P = 3$	0.1401	0.1402	0.1405
$P = 4$	0.1352	0.1353	0.1356
$P = 5$	0.1242	0.1321	0.1248
full ceramic	0.1107	0.1107	0.1110

FGM cantilever beam (with square-section)

Table 3 Shows the maximum rotation for the FGM cantilever beam according to various values of the power-law exponent. The results obtained show a good description of the mechanical behavior of the FGM beam in terms of rotation for all theories. It can be noted that the rotation of the full ceramic beam is lower than the full metal in both theories, while the FGM beam rotation is between the ceramic and metal beams.

The effect of restricted warping is known to be significant for a square-section subjected to torsion. In this section, a comparison of the results between SVBT and RBT are systematically made for the shear effects of the FGM beam. Fig. 17 illustrates a comparison between the shear stress field at the embedding and at the mid-span of homogeneous and FGM beams. We can observe the clear difference of the shear stress fields provided by the SVBT and RBT results at the embedding ($Z = 0$) in terms of shape and values, due to the enrichment of the displacement fields of the RBT (taking into account the edge effects), while the stress results presented by SVBT and RBT are consistent far from the embedding (mid-span of the beam).

Figs. 18 and 19 show the variation of the axial stress σ_{zz} along the beam for a point A close to the edge of the cross-section, and the variation of the shear stress for point B (the maximum shear point for the SVBT torsion) in the middle of the cross-section along the beam. Moving from the free end of the beam, we can observe an opposite relationship between the shear stresses and the axial stresses, where a decrease in shear follows an increase in axial stress or the reverse. These results show that the internal effect of the RBT propagates along the beam for this square-section, while the SVBT solution is no longer efficient to represent the central solution.

5 Conclusions

In the present paper, the bending-torsional behavour analysis of the functionally graded materials (FGMs) cantilever beams (I-section and square-section) has been studied using a refined 1D/3D beam theories (RBT and RBT*

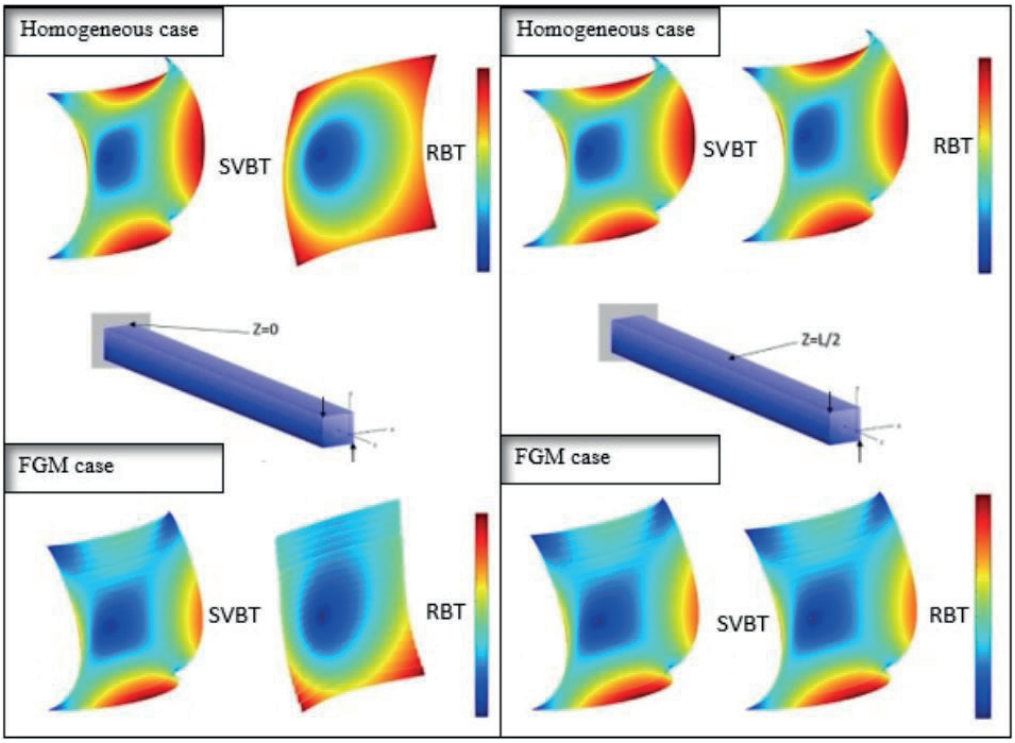

Fig. 17 Shear stress fields at $Z = 0$ and midspan $Z = L/2$. Comparison of SVBT and RBT results

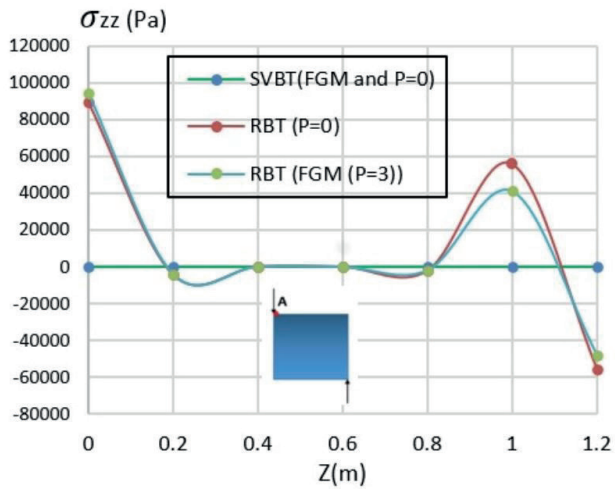

Fig. 18 Axial stress variation along the FGM and homogeneous ($P = 0$) beam for the point A

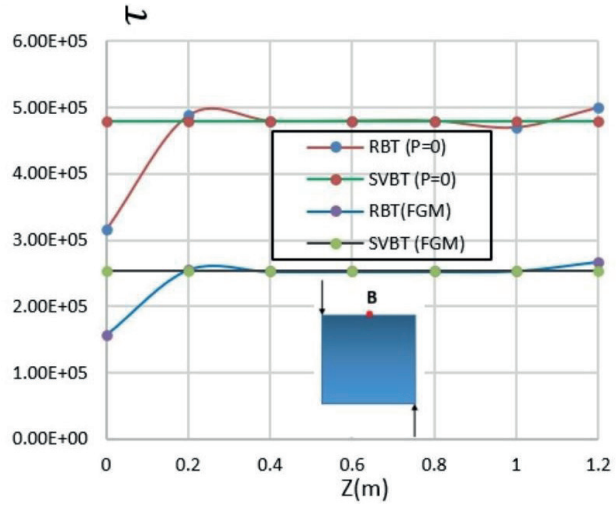

Fig. 19 shear stresses variation along the FGM and homogeneous ($P = 0$) beam for the point B

built on the 3D SV's solution). The enrichment of the displacement field includes the main deformation modes of the cross-section (Poisson's effects, out-of-plane deformations and distortions), These sectional modes are extracted from the associated 3D SV's solution for any given section and lead to a beam theory that really reflects the nature of the cross-section (shape and materials). which is important for FGM beams. In order to apply RBT/SV, a CSB package is used which has two tools, C-section and C-beam (complete each other). C-section calculates the mechanical characteristics of the cross-section by 2D FEM, then C-beam uses these mechanical characteristics to calculate the FGM beam by 1D FEM. Using the cross-section and beam problems presented in this paper, a 3D solution is given in more detail in terms of 3D displacements and deformations to analyze FGM cantilever beams.

The results of the refined 1D beam theories (RBT and RBT*) have shown that it is free of all the hypothesis of the classical beam and is applicable for an arbitrary cross-section. It is evident that RBT/SV is not only capable of describing the elastic structural performance of FGM beams, but also of providing a 3D solution in the major internal zone of the beam in terms of displacements and stresses (takes into account the edge effect). The axial stresses are the result of the bending stress and those induced by the torsional warping (actually the shear stress too, but it is clear that the torsional stress is more significant). As for SVBT, the axial stresses are those resulting from the typical SV's stresses in bending.

The shear stress field is completely different for the theories (shape and values) at embedding. For SVBT, the shear stresses are due to shear force and bending, while for RBT and RBT*, the inhibition stress resulted in a completely different shear field (degree of enrichment of cross-section strain modes). On the other hand, the results obtained by SVBT lead to a more flexible torsion behavior this is due to the fact that the embedding leaves the deformation of the cross-section free. The fact that this deformation may be blocked in RBT and RBT*, when compared to SVBT, to a stiffening of the torsional behavior (The rotation at the end is twice as small).

Acknowledgments

We would like to thank the Direction Générale de la Recherche Scientifique et du Développement Technologique (DGRSDT) through its Agence Thématique de Recherche Scientifique et Technologique (ATRST) for supporting this doctoral research, which is part of the research project number A01L02UN240120190001.

References

[1] Shen, H.-S. "Functionally Graded Materials, Nonlinear Analysis of Plates and Shells", CRC press, 2016. ISBN 9780367386016

[2] Reddy, J. N. "Analysis of functionally graded plates", International Journal for Numerical Methods in Engineering, 47(1–3), pp. 663–684, 2000. https://doi.org/doi: 10.1002/(SICI)1097-0207(20000110/30)47:1/3<663::AID-NME787>3.0.CO;2-8

[3] Murin, J., Aminbaghai, M., Hrabovsky, J., Gogola, R., Kugler, S. "Beam finite element for modal analysis of FGM structures", Engineering Structures, 121, pp. 1–18, 2016. https://doi.org/10.1016/j.engstruct.2016.04.042

[4] Yoon, K., Lee, P.-S., Kim, D.-N. "Geometrically nonlinear finite element analysis of functionally graded 3D beams considering warping effects", Composite Structures, 132, pp. 1231–1247, 2015. https://doi.org/10.1016/j.compstruct.2015.07.024

[5] Birman, V., Byrd, L. W. "Modeling and analysis of functionally graded materials and structures", Applied Mechanics Reviews, 60(1–6), pp. 195–216, 2007. https://doi.org/10.1115/1.2777164

[6] Lanc, D., Turkalj, G., Vo, T. P., Brnić, J. "Nonlinear buckling behaviours of thin-walled functionally graded open section beams", Composite Structures, 152, pp. 829–839, 2016. https://doi.org/10.1016/j.compstruct.2016.06.023

[7] Chakraborty, A., Gopalakrishnan, S., Reddy, J. N. "A new beam finite element for the analysis of functionally graded materials", International Journal of Mechanical Sciences, 45(3), pp. 519–539, 2003. https://doi.org/10.1016/S0020-7403(03)00058-4

[8] Wu, L., Wang, Q., Elishakoff, I. "Semi-inverse method for axially functionally graded beams with an anti-symmetric vibration mode", Journal of Sound and Vibration, 284(3–5), pp. 1190–1202, 2005. https://doi.org/10.1016/j.jsv.2004.08.038

[9] Rahmani, F., Kamgar, R., Rahgozar, R. "Finite element analysis of functionally graded beams using different beam theories", Civil Engineering Journal, 6(11), pp. 2086–2102, 2020. https://doi.org/10.28991/cej-2020-03091604

[10] Ying, J., Lü, C. F., Chen, W. Q. "Two-dimensional elasticity solutions for functionally graded beams resting on elastic foundations", Composite Structures, 84(3), pp. 209–219, 2008. https://doi.org/10.1016/j.compstruct.2007.07.004

[11] Barretta, R., Feo, L., Luciano, R. "Some closed-form solutions of functionally graded beams undergoing nonuniform torsion", Composite Structures, 123, pp. 132–136, 2015. https://doi.org/10.1016/j.compstruct.2014.12.027

[12] Giunta, G., Belouettar, S., Carrera, E. "Analysis of FGM beams by means of classical and advanced theories", Mechanics of Advanced Materials and Structures, 17(8), pp. 622–635, 2010. https://doi.org/10.1080/15376494.2010.518930

[13] Kadoli, R., Akhtar, K., Ganesan, N. "Static analysis of functionally graded beams using higher order shear deformation theory", Applied Mathematical Modelling, 32(12), pp. 2509–2525, 2008. https://doi.org/10.1016/j.apm.2007.09.015

[14] Kang, Y.-A., Li, X.-F. "Bending of functionally graded cantilever beam with power-law non-linearity subjected to an end force", International Journal of Non-Linear Mechanics, 44(6), pp. 696–703, 2009. https://doi.org/10.1016/j.ijnonlinmec.2009.02.016

[15] Li, L., Li, X., Hu, Y. "Nonlinear bending of a two-dimensionally functionally graded beam", Composite Structures, 184, pp. 1049–1061, 2018. https://doi.org/10.1016/j.compstruct.2017.10.087

[16] Kien, N. D., Gan, B. S. "Large deflections of tapered functionally graded beams subjected to end forces", Applied Mathematical Modelling, 38(11–12), pp. 3054–3066, 2014. https://doi.org/10.1016/j.apm.2013.11.032

[17] Sankar, B. V. "An elasticity solution for functionally graded beams", Composites Science and Technology, 61(5), pp. 689–696, 2001. https://doi.org/10.1016/S0266-3538(01)00007-0

[18] Benatta, M. A., Mechab, I., Tounsi, A., Adda Bedia, E. A. "Static analysis of functionally graded short beams including warping and shear deformation effects", Computational Materials Science, 44(2), pp. 765–773, 2008. https://doi.org/10.1016/j.commatsci.2008.05.020

[19] Nguyen, D. K., Gan, B. S., Le, T. H. "Dynamic Response of Non-Uniform Functionally Graded Beams Subjected to a Variable Speed Moving Load", Journal of Computational Science and Technology, 7(1), pp. 12–27, 2013. https://doi.org/10.1299/jcst.7.12

[20] Sindkhedkar, M., Jagtap, S., Shah, C., Palle, V. P. "Pharmaceutical Research in India: Current Status and Opportunities", Proceedings of the Indian National Science Academy, 4, pp. 829–842, 2019.

[21] Li, S.-R., Cao, D.-F., Wan, Z.-Q. "Bending solutions of FGM Timoshenko beams from those of the homogenous Euler-Bernoulli beams", Applied Mathematical Modelling, 37(10–11), pp. 7077–7085, 2013. https://doi.org/10.1016/j.apm.2013.02.047

[22] Nguyen, T.-T., Kim, N.-I., Lee, J. "Analysis of thin-walled open-section beams with functionally graded materials", Composite Structures, 138, pp. 75–83, 2016. https://doi.org/10.1016/j.compstruct.2015.11.052

[23] Yang, Y. Y. "Time-dependent stress analysis in functionally graded materials", International Journal of Solids and Structures, 37(51), pp. 7593–7608, 2000. https://doi.org/10.1016/S0020-7683(99)00310-8

[24] Şimşek, M. "Bi-directional functionally graded materials (BDFGMs) for free and forced vibration of Timoshenko beams with various boundary conditions", Composite Structures, 133, pp. 968–978, 2015. https://doi.org/10.1016/j.compstruct.2015.08.021

[25] Nguyen, H. N., Hong, T. T., Van Vinh, P., Van Thom, D. "An efficient beam element based on Quasi-3D theory for static bending analysis of functionally graded beams", Materials, 12(13), 2198, 2019. https://doi.org/10.3390/ma12132198

[26] Boutahar, Y., Lebaal, N., Bassir, D. "A refined theory for bending vibratory analysis of thick functionally graded beams", Mathematics, 9(12), 1422, 2021. https://doi.org/10.3390/math9121422

[27] Madenci, E. "A refined functional and mixed formulation to static analyses of fgm beams", Structural Engineering and Mechanics, 69(4), pp. 427–437, 2019. https://doi.org/10.12989/sem.2019.69.4.427

[28] Garg, A., Chalak, H. D., Chakrabarti, A. "Comparative study on the bending of sandwich FGM beams made up of different material variation laws using refined layerwise theory", Mechanics of Materials, 151, 103634, 2020. https://doi.org/10.1016/j.mechmat.2020.103634

[29] Demirbas, M. D., Caliskan, U., Xu, X., Filippi, M. "Evaluation of the bending response of compact and thin-walled FG beams with CUF Evaluation of the bending response of compact and thin-walled FG beams", Mechanics of Advanced Materials and Structures, 28(17), pp. 1755–1764, 2020. https://doi.org/10.1080/15376494.2019.1704951

[30] Zghal, S., Dammak, F. "Vibrational behavior of beams made of functionally graded materials by using a mixed formulation", Proceedings of the Institution of Mechanical Engineers, Part C: Journal of Mechanical Engineering Science, 234(18), pp. 3650–3666, 2020. https://doi.org/10.1177/0954406220916533

[31] Ziou, H., Guenfoud, M., Guenfoud, H. "A simple higher-order shear deformation theory for static bending analysis of functionally graded beams", Jordan Journal of Civil Engineering, 15(2), pp. 209–224, 2021.

[32] Nguyen, T.-T., Thang, P. T., Lee, J. "Flexural-torsional stability of thin-walled functionally graded open-section beams", Thin-Walled Structures, 110, pp. 88–96, 2017. https://doi.org/10.1016/j.tws.2016.09.021

[33] Guendouz, I., Guenfoud, H., Guenfoud, M., Khebizi, M., Elfatmi, R. "Bending-torsional behavior analysis using a refined beam theory", Academic Journal of Civil Engineering, 39(1), pp. 59–62, 2021. https://doi.org/10.26168/ajce.39.1.13

[34] Khebizi, M., Guenfoud, H., Guenfoud, M., El Fatmi, R. "Three-dimensional modelling of functionally graded beams using Saint-Venant's beam theory", Structural Engineering and Mechanics, 72(2), pp. 257–273, 2019. https://doi.org/10.12989/sem.2019.72.2.257

[35] Guenfoud, H., Ziou, H., Himeur, M., Guenfoud, M. "Analyses of a composite functionally graded material beam with a new transverse shear deformation function", Journal of Applied Engineering Science & Technology, 2(2), pp. 105–113, 2016.

[36] Hadji, L., Daouadji, T. H., Meziane, M. A. A., Tlidji, Y., Bedia, E. A. A. "Analysis of functionally graded beam using a new first-order shear deformation theory", Structural Engineering and Mechanics, 57(2), pp. 315–325, 2016. https://doi.org/10.12989/SEM.2016.57.2.315

[37] Ziou, H., Guenfoud, H., Guenfoud, M. "Numerical modelling of a Timoshenko FGM beam using the finite element method", International Journal of Structural Engineering, 7(3), pp. 239–261, 2016. https://doi.org/10.1504/IJSTRUCTE.2016.077719

[38] Guenfoud, H. "Modélisation par éléments finis spéciaux des structures en matériaux à gradient fonctionnel" (Modeling by special finite elements of structures in materials with functional gradient), PhD Thesis, University of Guelma, 2019.

[39] Alexraja, P. N. S., Vasirajab, N. "Graded Material Beam Using Finite Element Method", In: 2013 International Conference on Energy Efficient Technologies for Sustainability (ICEETS 2013), Nagercoil, India, 2013, pp. 267–273.

[40] Naccache, F., El Fatmi, R. "Buckling analysis of homogeneous or composite I-beams using a 1D refined beam theory built on Saint Venant's solution", Thin-Walled Structures, 127, pp. 822–831, 2018. https://doi.org/10.1016/j.tws.2018.02.028

[41] El Fatmi, R. "A refined 1D beam theory built on 3D Saint-Venant's solution to compute homogeneous and composite beams", Journal of Mechanics of Materials and Structures, 11(4), pp. 345–378, 2016. https://doi.org/10.2140/jomms.2016.11.345

[42] Naccache, F., El Fatmi, R. "Numerical free vibration analysis of homogeneous or composite beam using a refined beam theory built on Saint Venant's solution", Computers & Structures, 210, pp. 102–121, 2018. https://doi.org/10.1016/j.compstruc.2018.08.005

[43] El Fatmi, R., Ghazouani, N. "Higher order composite beam theory built on Saint-Venant's solution. Part-I: Theoretical developments", Composite Structures, 93(2), pp. 557–566, 2011. https://doi.org/10.1016/j.compstruct.2010.08.024

[44] Hong, K.-S., Chen, L.-Q., Pham, P.-T., Yang, X.-D. "Beam Model", In: Control of Axially Moving System, Springer, 2022, pp. 53–123. ISBN 978-981-16-2914-3 https://doi.org/10.1007/978-981-16-2915-0_3

[45] Şimşek, M. "Static Analysis of a Functionally Graded Beam Under a uniformly distributed load by Ritz method", International Journal of Engineering and Applied Sciences (IJEAS), 1(3), pp. 1–11, 2009.